

Long-Period Long-Duration Events Detected by the IRIS Community Wavefield Demonstration Experiment in Oklahoma: Tremor or Train Signals?

by Chenyu Li, Zefeng Li, Zhigang Peng, Chengyuan Zhang, Nori Nakata, and Tim Sickbert

ABSTRACT

In this study, we apply a recently developed local similarity method to detect long-period long-duration (LPLD) seismic events using 1-month continuous waveforms recorded by a nodal array from the Incorporated Research Institutions for Seismology (IRIS) community wavefield experiment in Oklahoma. The local similarity method detects seismic events by correlating waveforms at each station with its neighboring stations. Using this method, we visually identify 21 potential tremor-like LPLD events lasting more than 300 s during the 1-month period. However, with beamforming analysis, we find that the source locations and waveform characteristics of these events are consistent with train-generated seismic signals from the nearby Union Pacific railway. Additional evidence includes amplitude decay away from the railway track, and similarities in frequency-time contents with other confirmed traingenerated seismic signals. This case study highlights the need of dense-array observations to distinguish between natural and anthropogenic LPLD seismic signals.

Electronic Supplement: Table of detected train signals, figures of additional examples of possible train-generated seismic signals, relative energy across the array for possible long-period long-duration (LPLD) events, and daily stacked local similarity traces, and movie of earthquake sound.

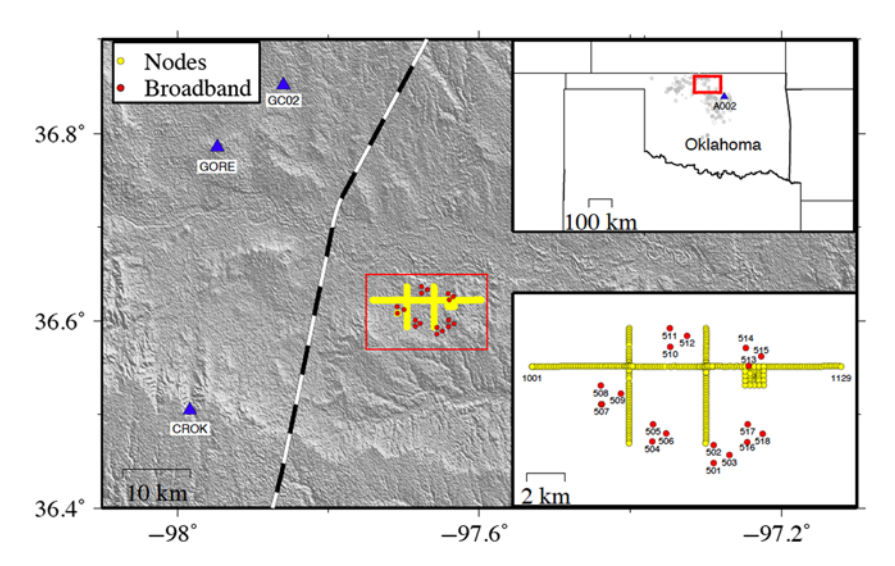
INTRODUCTION

Deep tectonic tremors (also known as nonvolcanic tremors) and low-frequency earthquakes (LFEs) are seismic events with low amplitudes, long periods, and long durations compared with regular earthquakes of similar sizes (Obara, 2002). They have been observed at major subduction zones and strike-slip fault systems around the Pacific Rim (Peng and Gomberg,

2010; Beroza and Ide, 2011; Schwartz, 2015; and references therein). Tectonic tremors and LFEs generally occur below the seismogenic zones where regular earthquakes occur, sometimes accompanied by geodetically observable slow-slip events (Rogers and Dragert, 2003; Obara *et al.*, 2004). Because they are extremely stress sensitive, they are essential for understanding deep fault structures and earthquake nucleation process (e.g., Obara and Kato, 2016; Chao *et al.*, 2017).

At shallower depths above the seismogenic zone, very lowfrequency earthquakes with characteristic periods of 10-50 s have been observed along several subduction zones (e.g., Ito and Obara, 2006; Walter et al., 2011; Hutchison and Ghosh, 2016). Recent studies with ocean-bottom seismometers and absolute pressure gauges also revealed long-duration tremor signals and slow-slip events in the shallow subduction-zone environments (Matsuzawa et al., 2015; Wallace et al., 2016; Araki et al., 2017). Shallow long-period long-duration (LPLD) tremor-like events have not been widely observed at major faults in continental settings, although episodic creep and slow-slip events have long been reported along several plateboundary faults that creep at shallow depths (Linde et al., 1996; Wei et al., 2013; Schwartz, 2015; Harris, 2017). On the other hand, similar LPLD events at shallower depths have been observed during slow-moving landslides and glaciers (Helmstetter and Garambois, 2010; Gomberg et al., 2011; Winberry et al., 2013), as well as during hydraulic fracturing operations in oil fields (Kanamori and Hauksson, 1992; Das and Zoback, 2013a,b; Hu et al., 2017).

The detection and analysis of LPLD events at shallow depths could be affected by seismic signals generated by other natural or anthropogenic sources. For example, regional moderate-size earthquakes could be mistakenly identified as LPLD events (Caffagni *et al.*, 2015; Zecevic *et al.*, 2016; Chen *et al.*, 2018). Another source of contamination is human activities, such as injection operations, nearby road traffics, trains,



▲ Figure 1. Map of the study region in north central Oklahoma. Stations in the small box are the Incorporated Research Institutions for Seismology (IRIS) community wavefields demonstration experiment (YW network). The thick black and white line is the railway nearby, and triangles are broadband stations operated by Oklahoma Geological Survey (OGS). (Upper right inset) Location of the study region in the larger map of Oklahoma and nearby states. Gray dots are OGS catalog events during the study period. Station A002 is deployed by Oklahoma State University and is \sim 3 km from a different railway. (Lower right inset) A zoom-in map showing the detailed station geometry of the YW network. The color version of this figure is available only in the electronic edition.

or even air traffics (Riahi and Gerstoft, 2015; Li et al., 2018; Meng and Ben-Zion, 2018). Certain types of sources are relatively easy to identify. For example, helicopters and airplanes typically produce seismic signals with clear Doppler effects, mimicking gliding harmonic tremors during or preceding volcanic eruptions (Hotovec et al., 2013; Eibl et al., 2015; Meng and Ben-Zion, 2018). However, it is difficult to distinguish between seismic signals generated by trains and tectonic tremors during slow-slip events in several aspects: (1) they both have long durations, lasting several to several tens of minutes; (2) their dominant frequencies are in the relatively long period of 1-10 Hz (in comparison with microearthquakes of similar amplitudes); (3) sometimes they have harmonic frequency bands; and (4) their sources move at a speed of several tens of kilometers per hour (e.g., Shelly et al., 2011; Fuchs et al., 2017; Hutchison and Ghosh, 2017). Hence, in search of LPLD tremor-like events, it is important to rule out potential contaminations of train-generated signals and other anthropogenic sources.

In this work, we present another case study of possible train-related LPLD tremor-like events recorded by the Oklahoma wavefield experiment nodal array (Sweet et al., 2018). The significant increase in small- to moderate-size earthquakes in Oklahoma since 2009 was mostly attributed to wastewater injections after shale gas developments in that region (Ellsworth, 2013; Keranen et al., 2014). Motivated by recent laboratory and field observations of tremor-type events during aseismic slip induced by fluid injections (Zigone et al., 2011;

Guglielmi et al., 2015; Hu et al., 2017), our initial target was to identify potential tremor-like signals recorded by the dense nodal array in Oklahoma (Li et al., 2017). In the following sections, we first apply a recently developed local similarity method (Li et al., 2018) to identify LPLD tremor-like signals and then analyze their frequency content, wavespeed, and direction. We find that these LPLD signals are likely seismic footprints of the traveling train to the west of the array. We also present a catalog of possible train-related events during the 1-month recording, which can be used as a reference for other studies with similar targets or the same dataset.

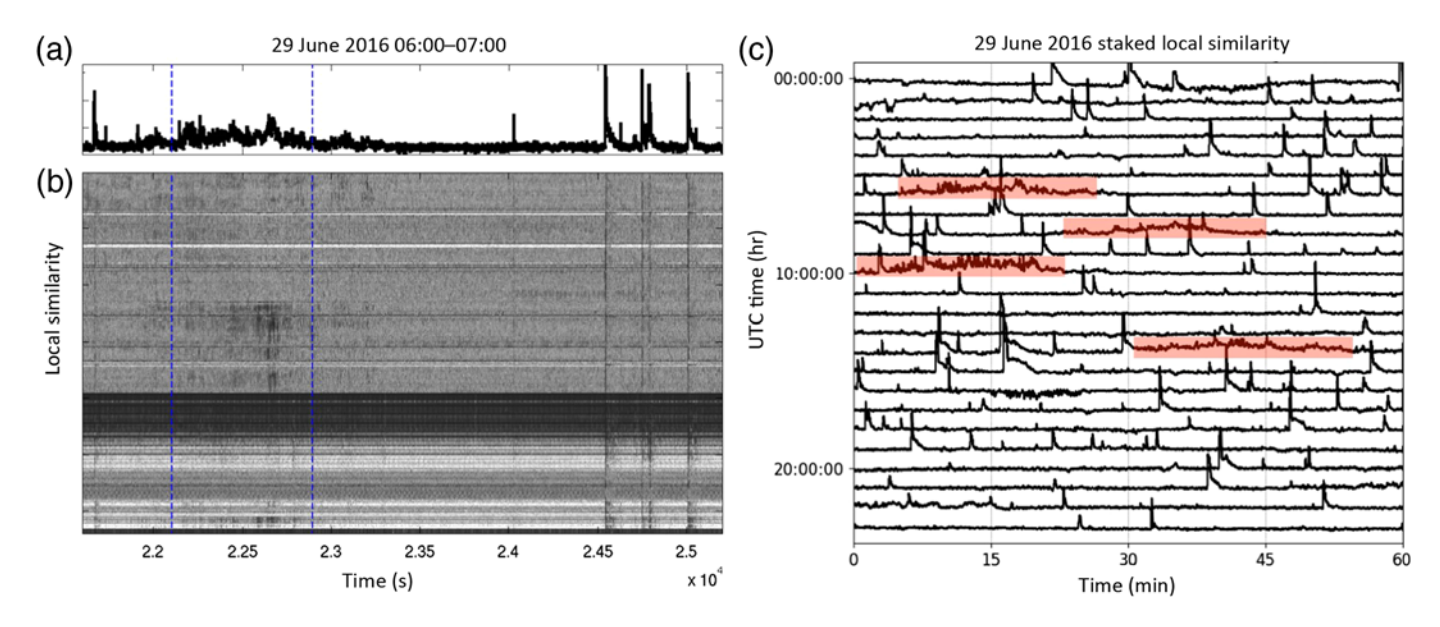
DATA AND METHOD

The IRIS community wavefield demonstration experiment was deployed near the town of Lamont in north central Oklahoma, and the ultra-dense seismic array was recorded from 22 June to 20 July 2016 (Fig. 1). This array includes 361 three-component nodal sensors deployed as 3 lines, a 7-layer nested gradiometer subarray and 18 broadband stations collocated with some infrasound stations; a near northsouth-strike railway track is located about

10 km to the west of the dense array (Fig. 1). We use all nodal stations for the initial event detection and the broadband stations for subsequent analysis of the detected signals.

We use the local similarity method (Li et al., 2018) to detect seismic events recorded by this large-N array. The local similarity of a single station is defined as the stacked cross correlation (CC) between the record of this station and those of its four nearest neighboring stations. This is based on the simple fact that interstation spacing in this array is so small that the waveforms on nearby stations are very similar. After calculating the local similarities for all stations, we stack them to obtain a mean local similarity trace. For short aperture arrays (e.g., < 20 km), the maximum time shift across the array is so small (e.g., less than a few seconds) that direct stacking of local similarity traces can be still constructive. After CC of nearby waveforms and stacking of local similarity traces, incoherent noise is suppressed, and coherent signals are enhanced. Because this method does not require any prior information about the target signals, it can be used to detect unknown types of events.

Our detailed analysis procedure is described later. We first download all the waveforms recorded by the nodal stations in the wavefield experiment (network code YW) from the IRIS Data Management Center (DMC). We filter the data in 5–10 Hz and downsample by a factor of 10 (from 250 to 25 Hz); this frequency range is chosen to suppress regional and teleseismic signals and higher frequency local noises (Li et al., 2018). Next, we apply the local similarity method to the preprocessed data. We use a 1-s time window with moving step of three resampled



▲ Figure 2. (a) One hour mean local similarity trace of all the nodal stations during 29 June 2016 06:00–07:00. The visually identified long-period long-duration (LPLD) event is marked within two dashed lines. The vertical spikes mark local microearthquakes. (b) Local similarity trace at individual station. (c) Hourly mean local similarity traces on 29 June 2016. Four visually identified LPLD events are marked in small shaded boxes. The color version of this figure is available only in the electronic edition.

data points to calculate sliding window normalized CC between two stations. The CC at a given time step is the searched maximum value over a time-window length corresponding to the arrival-time difference between the two stations. We then average the CC traces of one master station with its four nearest neighbors to obtain a single local similarity trace for the master station and followed by stacking the local similarity traces for all the stations. Finally, we visually inspect the mean local similarity traces and identify long-duration events that are clearly above background noises.

After identifying these LPLD events, we apply a beamforming technique to the 7-layer nested gradiometer subarray to obtain the back azimuths and incidence angles of these events (Rost and Thomas, 2002; Helffrich *et al.*, 2013; Sun *et al.*, 2015). We use this gradiometer subarray for the beamforming analysis because its small aperture (< 2 km) can satisfy the plane-wave assumption. Following Sun *et al.* (2015), we compute the broadband frequency—wavenumber (BBFK) spectra of band-pass 2–8 Hz filtered waveforms using the BBFK command in Seismic Analysis Code and obtain the wavenumber and back azimuth with a 120-s time moving window with 50% overlap (i.e., shifting 60 s each time).

RESULTS

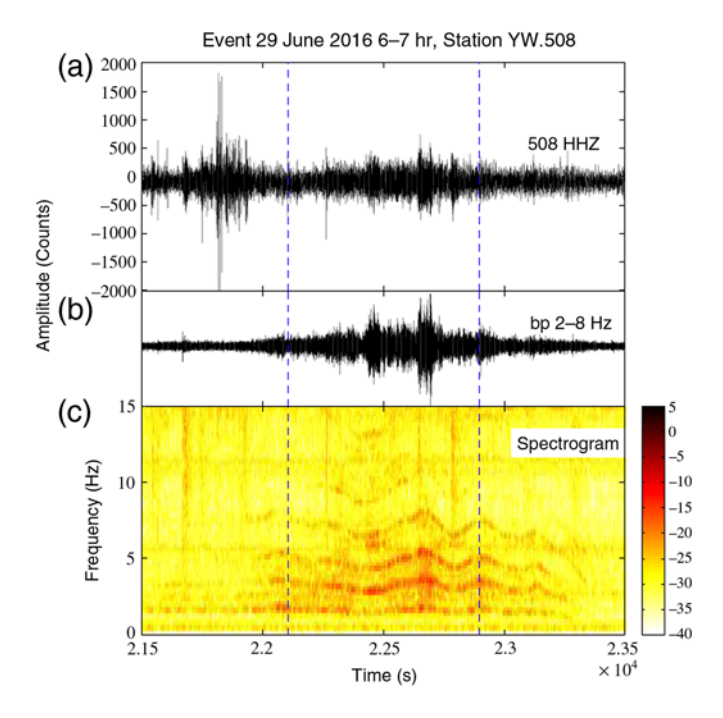
During the 1-month recording period, we visually identify 21 tremor-like events. Figure 2 shows an example of mean and individual local similarity traces on 29 June 2016 06:00–07:00 UTC (Julian day 181). We can clearly observe several sharp spikes that are local earthquakes, most of which matched with events listed in both the Oklahoma Geological Survey (OGS) catalog and newly detected microearthquakes with

the same dataset (Nakata, 2017). In addition, there is an ~1000-s LPLD event with local similarity slightly higher than the background level (Fig. 2a). The individual local similarity traces (Fig. 2b) also show such long-duration event in the first half hour. A total of four LPLD events have been identified on that day (Fig. 2c), together with many earthquake-like signals.

Next, we compute the spectrogram of the same LPLD event recorded by the broadband station 508. In addition to a few vertical stripes, the majority of the tremor-like signals show clear harmonic frequency contents (Fig. 3). The corresponding sound by speeding up the playback 100 times (Kilb et al., 2012) can be found in

Movie S1 (available in the electronic supplement to this article). We observe a gradual increase and decrease in frequency over time, which is also shown for other events and recorded by the nodal station for the same event (© Fig. S1). Such harmonic frequency contents and temporal variations are similar to other confirmed cases of train-generated signals (Chen et al., 2004; Quiros et al., 2016; Fuchs et al., 2017) and a broadband seismic station deployed ~3 km of a different railway track in Morrison, Oklahoma (© Fig. S1).

We then obtain the back azimuth and wavenumbers from the beamforming analysis on 29 June 2016 05:00–07:00 (Fig. 4). The time window corresponding to the LPLD event delineates a moving source with back azimuth changing from 305° to 250°. The frequency–wavenumber (f-k) amplitude (beam power) contour of several time windows during the LPLD event can be found in © Figure S2. Based on the relationship between wavenumber k and horizontal slowness p, we estimate the apparent velocity $c_{\rm app} = f/k = 1.36 \ {\rm km/s}$ in which $f=3.5 \ {\rm Hz}$ is the dominant frequency and



▲ Figure 3. (a) Raw waveform, (b) 2-8 Hz band-pass filtered, (c) spectrogram of the same LPLD event shown in Figure 2a and recorded by the broadband station 508. The color version of this figure is available only in the electronic edition.

k = 2.58 cycle/km is the wavenumber obtained from peak BBFK spectra (Helffrich et al., 2013). Furthermore, we estimate the incident angle $\theta = 61.92^{\circ}$ by $c_{\rm app} = c/\sin\theta$, and here we assume c = 1.2 km/s, an average surface shear-wave velocity in Oklahoma (Fletcher et al., 2006). The relatively large incident angle suggests that this LPLD event is likely from a shallow source.

Figure 5a shows the 2- to 8-Hz band-pass filtered waveform of the LPLD event recorded by selected stations from the horizontal seismic line with a constant spatial interval. The amplitudes of the tremor-like signals decay systematically from west to east. To better quantify whether the signals are originated from passing trains on the nearby railway, we compute the sum of the squared velocity between 22,140 and 22,980 s relative to 29 June 2016 00:00:00 (29 June 2016 06:09:00-06:23:00), which are the starting and ending time obtained from beamforming analysis, and use it as a proxy for radiated seismic energy. As shown in Figure 5b, the squared velocity sum decay roughly follows a log-linear relationship with d, in which d is the shortest distance from the railway track. We compare the decay rate with body-wave decays of surface sources $A = d^{-3/2} \exp(-\frac{\pi f d}{Q \nu})$, where we assume f = 5 Hz, v = 1.2 km/s, and the term $\exp(-\frac{\pi f d}{Q v})$ is a result of attenuation. We find that the attenuation factor Q between 50 and 150 provides a good fit to the curve (Fig. 5b). The cumulative energies of two events at all nodal stations are shown in E Figure S3. Figure 5 and © Figure S3 show that stations in the western side have generally higher energy than the eastern

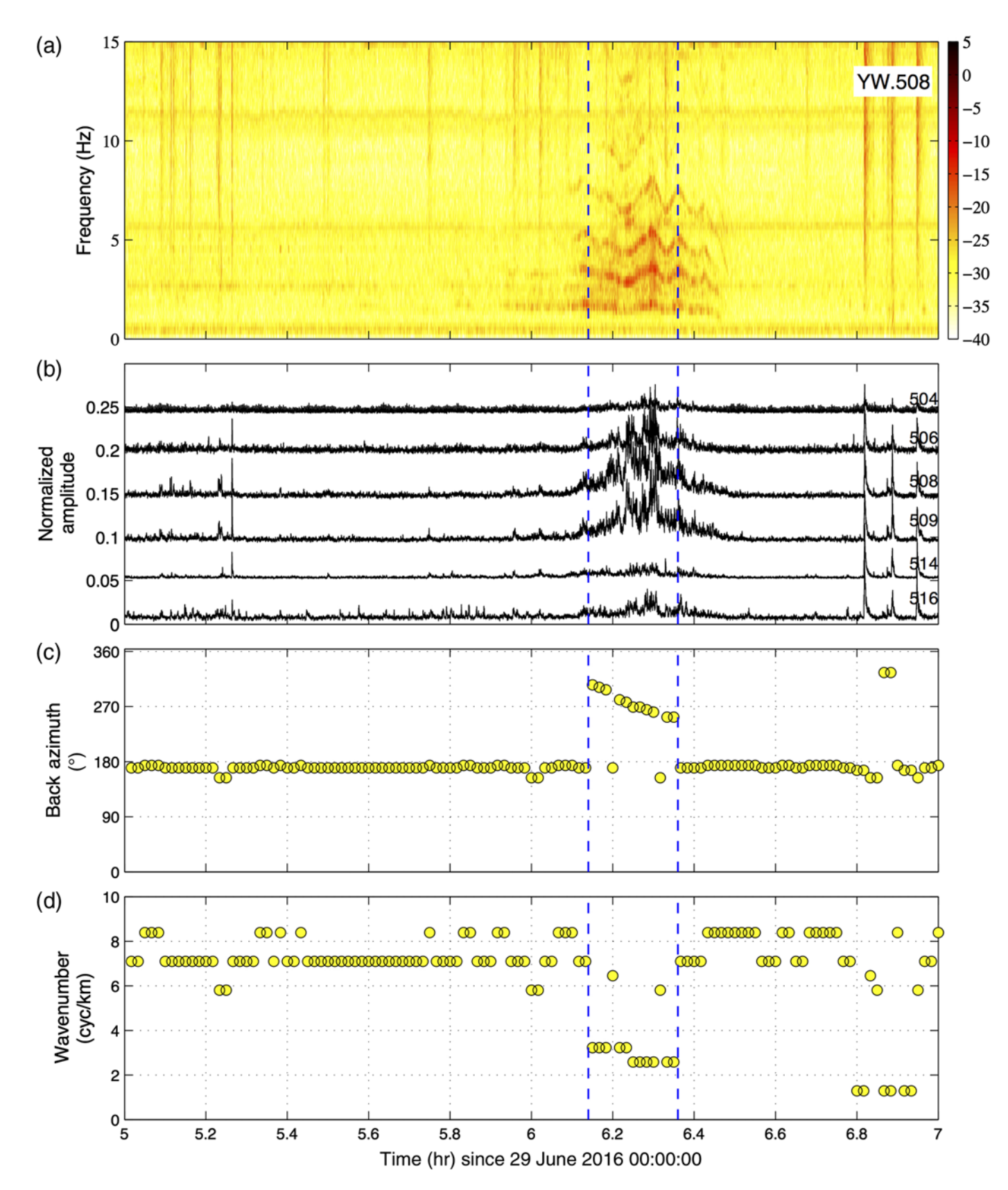
side, consistent with westward location of the railway. Generally, the signals become visually undetectable on stations with distances larger than ~15 km from the railway. To demonstrate that the moving source has little effect on the decaying of energy, we use a smaller time window of 120 s (with 60-s overlap) and recalculate the normalized energy with distances. As shown in (E) Figure S4, we do not observe any clear change in the decay rate with time, suggesting that the moving source did not affect this calculation.

DISCUSSION

Recent studies have shown that hydraulic-fracture operations could induce LPLD tremor-like events (Das and Zoback, 2013a,b; Hu et al., 2017). Although some LPLD events in their studies might be small regional earthquakes (Caffagni et al., 2015; Chen et al., 2018), the characteristics of the LPLD events observed in this study are different from any of them. For example, the duration of our detected LPLD events is more than 300 s, much longer than the typical duration of 30-60 s for the LPLDs in the other studies. Furthermore, whereas the dominant frequency of our LPLD events is less than 10 Hz, the LPLD events during hydraulic fracturing can reach up to 60–100 Hz (Das and Zoback, 2013a,b; Hu et al., 2017; Chen et al., 2018). These differences suggest that the source mechanisms of LPLD events observed in this study are different from recent observations near hydraulic fracturing sites.

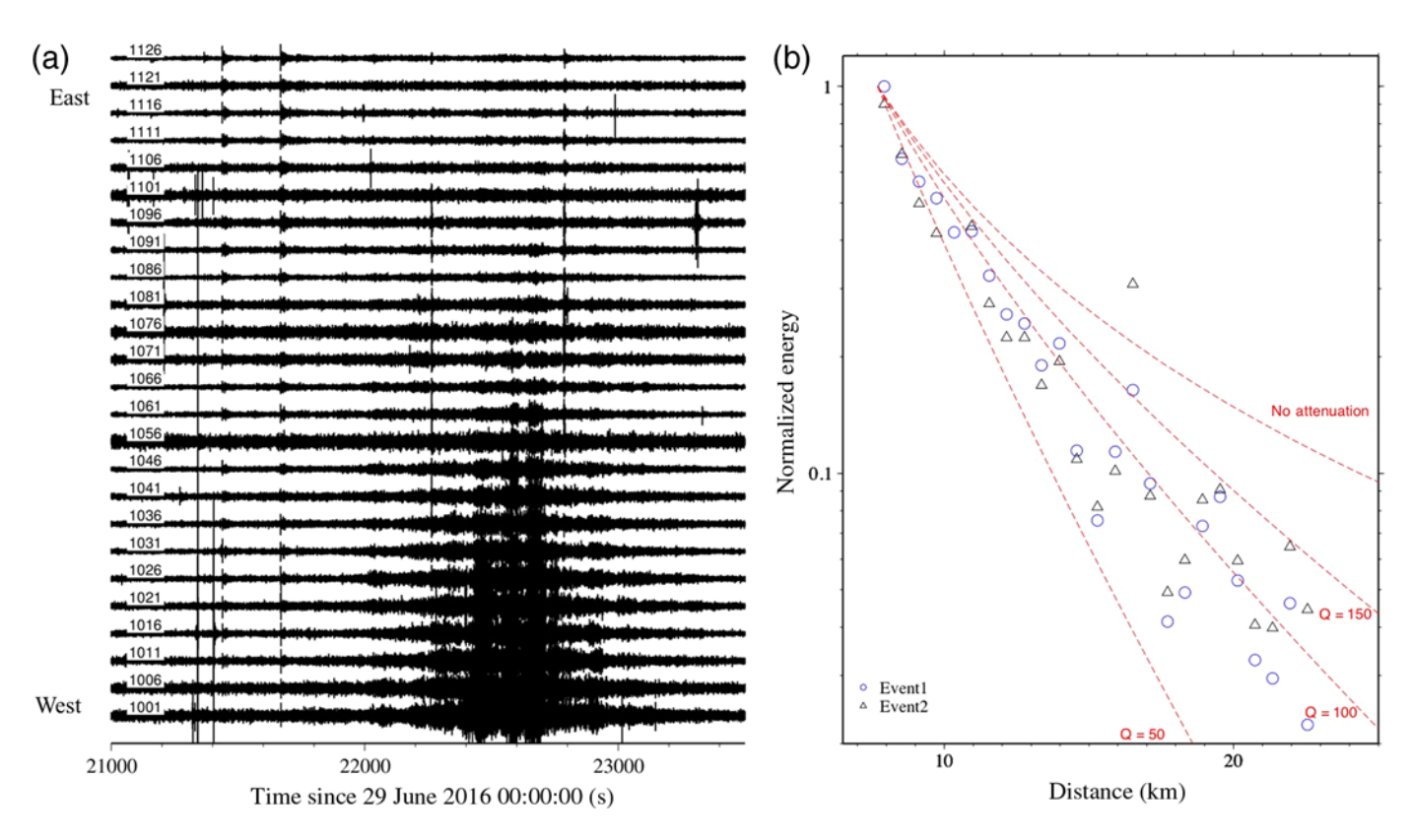
Detailed analysis of the waveforms and spectrograms of these LPLD events revealed that they are seismic footprints of traveling trains along a Union Pacific (UP) railway 10-20 km to the west of the array. The first supporting evidence is that the spectrogram of the LPLD event shows harmonic frequency bands and the Doppler effect, which is a typical feature for train signals (Chen et al., 2004; Quiros et al., 2016). We note that the harmonic frequency bands in other studies are much higher, which is likely due to the much longer source-receiver distance (~10 km) in this work than the distances in their studies (~300 m). Fuchs et al. (2017) suggested that track or wheel irregularities and static axle load are main mechanisms of vibrations generated by trains. Whereas wheel irregularities represent moving source and would have Doppler effect, axle load is quasi-static and explains constant spacing between spectral lines. The overtones with increasing and decreasing frequencies and spectral lines with constant spacing observed in our study could be a combination of multiple wheel regularities and axle loads.

The beamforming analysis on the ultra-dense gradiometer subarray shows moving sources from north to south, west of the subarray for most LPLD events, and 1-2 events moving from south to north, both consistent with the azimuths of the railway. Assuming that the source is on the railway, we estimate the source to move at a speed of ~80 km/hr, which is also comparable to a typical freight train speed. Unfortunately, the detailed schedule on the UP railway is not openly available at this stage. Hence, we cannot confirm our observation with known train schedule. Comparison with seismic data recorded



▲ Figure 4. An example showing the broadband frequency—wavenumber (BBFK) array analysis for the same LPLD event as shown in Figure 2a. (a) Spectrogram, (b) 2- to 8-Hz band-pass filtered envelope function, (c) back azimuth, (d) wavenumber of waveforms during 29 June 2016 05:00—07:00. The approximate time window of LPLD event is marked as vertical dashed lines. The color version of this figure is available only in the electronic edition.

1656 Seismological Research Letters Volume 89, Number 5 September/October 2018



▲ Figure 5. (a) Band-pass filtered 2- to 8-Hz waveform of same event as in Figure 2a recorded by nodal stations in the horizontal seismic line with an equal station spacing. (b) Normalized energy versus distance from the train track for two LPLD events showing similar decay across the array. The color version of this figure is available only in the electronic edition.

by stations very close to the railway would also provide additional information about the passage of train signals and the decay of seismic signals with distances.

In regions where seismic arrays are exposed to heavy cultural noises (e.g., trains, highways, helicopters, wind turbines), it is possible that the corresponding seismic signals might be mislabeled as natural events, such as LPLD tremor events or microearthquakes (Riahi and Gerstoft, 2015; Meng and Ben-Zion, 2018). Hence, we need to be cautious when analyzing seismic data in these regions (e.g., Hutchison and Ghosh, 2017). There are also some other types of anthropogenic noises in our study region. For example, the beamforming shows a constant back azimuth around 180°, and we believe this is from noise of a nearby wind farm located to the south of the array (Stammler and Ceranna, 2016). We rule out the possibility that our detected LPLD events are from signals generated by wind turbines for the following reasons: the location of LPLD events start from northwest to the ultra-dense array, which is different from the locations of wind turbines. The occurrence time of the LPLD events did not show any correlation with the hourly wind speed. In addition, the wind turbines are evenly distributed from west to east, so it is not likely to cause a higher cumulative energy on the western part of the array.

Finally, the observation of energy is compatible with the assumption that the source of the signal is from the vibration of trains on the nearby railway. The decay rate of energy across

the linear array perpendicular to the railway fits well with bodywave decay considering near-surface attenuation from sediments. In addition, we did not find any events with higher energy in the eastern side of the array, indicating the signals persistently come from the west.

CONCLUSIONS

In this study, we detected 21 LPLD tremor-like events in Oklahoma from seismic data collected by the IRIS community wavefield experiment array. Our subsequent analysis revealed that they are most likely generated by moving trains along a nearby railway rather than generated by slow slip induced by hydraulic fracturing or wastewater injections. We came up with a catalog of train-related LPLD events identified with both local similarity and beamforming methods and the stacked local similarity trace for all 30 days (© Table S1, Figs. S5–S7). These possible train-related signals could be used as a potential labeled dataset for future automatic detection and classification of similar signals in this and other regions.

DATA AND RESOURCES

Seismic data used in this study are collected by the Incorporated Research Institutions for Seismology (IRIS) community wavefield experiment in Oklahoma and are open to public in

the IRIS Data Management Center (DMC; http://ds.iris.edu/mda/YW?timewindow=2016-2016, last accessed June 2018).

■

ACKNOWLEDGMENTS

The authors appreciate Incorporated Research Institutions for Seismology (IRIS) for deployment of the IRIS community wavefield experiment in Oklahoma and making the data available to public. The authors thank Heather Deshon and Mike Brudzinski for pointing out potential train-generated tremorlike signals at the 2017 Eastern Section of Seismological Society of America Annual Meeting in Norman, Oklahoma. The authors appreciate Editor Brandon Schmandt, Abhijit Ghosh, and two anonymous reviewers for their constructive suggestions to improve this article. This article has benefitted from the valuable advice and help from Kevin Chao in Northwestern University, U.S.A., and Wei-fang Sun in National Dong Hwa University, Taiwan. C. Li and Z. Peng are supported by National Science Foundation (NSF) Grants EAR-1551022 and EAR-1818611.

REFERENCES

- Araki, E., D. M. Saffer, A. J. Kopf, L. M. Wallace, T. Kimura, Y. Machida, S. Ide, E. Davis, and, and IODP Expedition 365 shipboard scientists (2017). Recurring and triggered slow slip events near the trench at the Nankai Trough subduction megathrust, *Science* 356, 1157–1160.
- Beroza, G. C., and S. Ide (2011). Slow earthquakes and nonvolcanic tremor, *Annu. Rev. Earth Planet. Sci.* 39, 271–296
- Caffagni, E., D. Eaton, M. Van der Barn, and J. P. Jones (2015). Regional seismicity: A potential pitfall for identification of long-period and long-duration events, *Geophysics* 80, no. 1, doi: 10.1190/geo2014-0382.1.
- Chao, K., Z. Peng, Y.-J. Hsu, K. Obara, C. Wu, K.-E. Ching, S. van der Lee, H.-C. Pu, P.-L. Leu, and A. Wech (2017). Temporal variation of tectonic tremor activity in southern Taiwan around the 2010 M_L6.4 Jiashian earthquake, J. Geophys. Res. 122, doi: 10.1002/ 2016JB013925.
- Chen, H., F. Niu, Y. Tang, and K. Tao (2018). Toward the origin of long-period long-duration seismic events during hydraulic fracturing treatment: A case study in the shale play of Sichuan Basin, China, *Seismol. Res. Lett.* **89**, 1075–1083, doi: 10.1785/0220170270.
- Chen, Q., L. Li, G. Li, L. Chen, W. Peng, Y. Tang, Y. Chen, and F. Wang (2004). Seismic features of vibration induced by train, *Acta Seismol. Sinica* 17, 715–724, doi: 10.1007/s11589-004-0011-7.
- Das, I., and M. D. Zoback (2013a). Long-period, long-duration seismic events during hydraulic stimulation of shale and tight-gas reservoirs —Part 1: Waveform characteristics, *Geophysics* 78, no. 6, doi: 10.1190/geo2013-0164.1.
- Das, I., and M. D. Zoback (2013b). Long-period, long-duration seismic events during hydraulic stimulation of shale and tight-gas reservoirs —Part 2: Locations and mechanisms, *Geophysics* 78, no. 6, doi: 10.1190/geo2013-0165.1.
- Eibl, E. P. S., I. Lokmer, C. J. Bean, E. Akerlie, and K. S. Vogfjörd (2015). Helicopter vs. volcanic tremor: Characteristic features of seismic harmonic tremor on volcanoes, *J. Volcanol. Geoth. Res.* 304, 108–117, doi: 10.1016/j.jvolgeores.2015.08.002.
- Ellsworth, W. (2013). Injection-induced earthquakes, *Science* **341**, available at http://www.sciencemag.org/content/341/6142/1225942 (last accessed July 2013).
- Fletcher, J. B., P. Spudich, and L. M. Baker (2006). Rupture propagation of the 2004 Parkfield, California, earthquake from observations at

- the UPSAR, *Bull. Seismol. Soc. Am.* **96**, no. 4B, S129–S142, doi: 10.1785/0120050812.
- Fuchs, F., G. Bokelmann, and the AlpArray Working Group (2017). Equidistant spectral lines in train vibrations, Seismol. Res. Lett. 89, no. 1, 56–66, doi: 10.1785/0220170092.
- Gomberg, J., W. Schulz, P. Bodin, and J. Kean (2011). Seismic and geodetic signatures of fault slip at the Slumgullion landslide natural laboratory, *J. Geophys. Res.* 116, no. B09404, doi: 10.1029/2011JB008304.
- Guglielmi, Y., F. Cappa, J. P. Avouac, P. Henry, and D. Elsworth (2015). Seismicity triggered by fluid injection-induced aseismic slip, *Science* 348, no. 6240, 1224–1226.
- Harris, R. A. (2017). Large earthquakes and creeping faults, *Rev. Geophys.* **55**, 169–198, doi: 10.1002/2016RG000539.
- Helffrich, G., J. Wookey, and I. Bastow (2013). The Seismic Analysis Code: A Primer and User's Guide, Cambridge University Press, New York, New York, 102–106.
- Helmstetter, A., and S. Garambois (2010). Seismic monitoring of Séchilienne rockslide (French Alps): Analysis of seismic signals and their correlation with rainfalls, *J. Geophys. Res.* **115**, F03016, doi: 10.1029/2009JF001532.
- Hotovec, A. J., S. G. Prejean, J. E. Vidale, and J. Gomberg (2013). Strong gliding harmonic tremor during the 2009 eruption of Redoubt volcano, *J. Volcanol. Geoth. Res.* **259**, no. 1, 89–99.
- Hu, H., A. Li, and R. Zavala-Torres (2017). Long-period long-duration seismic events during hydraulic fracturing: Implications for tensile fracture development, *Geophys. Res. Lett.* 44, 4814–4819, doi: 10.1002/2017GL073582.
- Hutchison, A. A., and A. Ghosh (2016). Very low frequency earthquakes spatiotemporally asynchronous with strong tremor during the 2014 episodic tremor and slip event in Cascadia, *Geophys. Res. Lett.* 43, no. 13, 6876–6882.
- Hutchison, A. A., and A. Ghosh (2017). Ambient tectonic tremor in the San Jacinto fault, near the Anza Gap, detected by multiple mini seismic arrays, *Bull. Seismol. Soc. Am.* 107, no. 5, 1985–1993.
- Ito, Y., and K. Obara (2006). Dynamic deformation of the accretionary prism excites very low frequency earthquakes, *Geophys. Res. Lett.* **33**, L02312, doi: 10.1029/2005GL025270.
- Kanamori, H., and E. Hauksson (1992). A slow earthquake in the Santa Maria Basin, California, Bull. Seismol. Soc. Am. 82, 2087–2096.
- Keranen, K. M., H. M. Savage, G. A. Abers, and E. S. Cochran (2014). Potentially induced earthquakes in Oklahoma, USA: Links between wastewater injection and the 2011 $M_{\rm w}$ 5.7 earthquake sequence, Geology 41, no. 6, 699–702, doi: 10.1130/G34045.1.
- Kilb, D, Z. Peng, D. Simpson, A. Michael, M. Fisher, and D. Rohrlick (2012). Listen, watch, learn: Seissound video product, Seismol. Res. Lett. 83, no. 2, 281–286, doi: 10.1785/gssrl.83.2.281.
- Li, C., Z. Li, Z. Peng, C. Zhang, N. Nakata, K. Chao, and T. Sickbert (2017). Detecting micro-seismicity and long-duration tremor-like events from the Oklahoma wavefield experiment, 2017 AGU Fall Meeting, New Orleans, Louisiana, 11–15 December 2017.
- Li, Z., Z. Peng, D. Hollis, L. Zhu, and J. McClellan (2018). Highresolution seismic event detection using local similarity for large-N arrays, Sci. Rep. 8, 1646, doi: 10.1038/s41598-018-19728-w.
- Linde, A. T., M. T. Gladwin, M. J. S. Johnston, R. L. Gwyther, and R. G. Bilham (1996). A slow earthquake sequence on the San Andreas fault, *Nature* 383, 65–68.
- Matsuzawa, T., Y. Asano, and K. Obara (2015). Very low frequency earth-quakes off the Pacific coast of Tohoku, Japan. *Geophys. Res. Lett.* **42**, 4318–4325, doi: 10.1002/2015GL063959.
- Meng, H., and Y. Ben-Zion (2018). Characteristics of airplanes and helicopters recorded by a dense seismic array near Anza California, *J. Geophys. Res.* doi: 10.1029/2017JB015240.
- Nakata, N. (2017). Data mining of IRIS wavefield experiment in Oklahoma, *Seismol. Res. Lett.* **88**, no. 2B, 615–616.
- Obara, K. (2002). Nonvolcanic deep tremor associated with subduction in southwest Japan, *Science* **296**, 1679–1681, doi: 10.1126/science.1070378.

- Obara, K., and A. Kato (2016). Connecting slow earthquakes to huge earthquakes, Science 353, no. 6296, 253-257, doi: 10.1126/science.aaf1512.
- Obara, K., H. Hirose, F. Yamamizu, and K. Kasahara (2004). Episodic slow slip events accompanied by non-volcanic tremors in southwest Japan subduction zone, Geophys. Res. Lett. 31, L23602, doi: 10.1029/2004GL020848.
- Peng, Z., and J. Gomberg (2010). An integrated perspective of the continuum between earthquakes and slow-slip phenomena, Geophys. Res. Lett. 3, 599-607, doi: 10.1038/ngeo940.
- Quiros, D. A., L. D. Brown, and D. Kim (2016). Seismic interferometry of railroad induced ground motions: Body and surface wave imaging, Geophys. J. Int. 205, no. 1, 301-313, doi: 10.1093/gji/ggw033.
- Riahi, N., and P. Gerstoft (2015). The seismic traffic footprint: Tracking trains, aircraft, and cars seismically, Geophys. Res. Lett. 42, doi: 10.1002/2015GL063558.
- Rogers, G., and H. Dragert (2003). Episodic tremor and slip on the Cascadia subduction zone: The chatter of silent slip, Science 300, no. 5627, 1942-1943.
- Rost, S., and C. Thomas (2002). Array seismology: Methods and applications, Rev. Geophys. 40, no. 3, 2-1-2-27, doi: 10.1029/2000RG000100.
- Schwartz, S. Y. (2015). Episodic aseismic slip at plate boundaries, in The Treatise on Geophysics, Second Ed., G. Schubert (Editor-in-Chief), Elsevier, Oxford, United Kingdom, 445-465.
- Shelly, D. R., Z. Peng, D. P. Hill, and C. Aiken (2011). Triggered creep as a possible mechanism for delayed dynamic triggering of tremor and earthquakes, Nature Geosci. doi: 10.1038/NGEO1141.
- Stammler, K., and L. Ceranna (2016). Influence of wind turbines on seismic records of the Gräfenberg array, Seismol. Res. Lett. 87, no. 5, 1075-1081, doi: 10.1785/0220160049.
- Sun, W.-F., Z. Peng, C.-H. Lin, and K. Chao (2015). Detecting deep tectonic tremor in Taiwan with a dense array, Bull. Seismol. Soc. Am. 105, no. 3, 1349-1358, doi: 10.1785/0120140258
- Sweet, J. R., K. R. Anderson, S. Bilek, M. Brudzinski, X. Chen, H. DeShon, C. Hayward, M. Karplus, K. Keranen, C. Langston, et al. (2018). A community experiment to record the full seismic wavefield in Oklahoma, Seismol. Res. Lett. doi: 10.1785/0220180079.
- Wallace, L. M., S. C. Webb, Y. Ito, K. Mochizuki, R. Hino, S. Henrys, S. Schwartz, and A. Sheehan (2016). Slow slip near the trench at the Hikurangi subduction zone, New Zealand, Science 352, no. 6286, 701-704, doi: 10.1126/science.aaf2349.
- Walter, J. I., S. Y. Schwartz, J. M. Protti, and V. Gonzalez (2011). Persistent tremor within the northern Costa Rica seismogenic zone, Geophys. Res. Lett. 38, L01307, doi: 10.1029/2010GL045586.
- Wei, M., Y. Kaneko, Y. Liu, and J. McGuire (2013). Episodic fault creep events in California controlled by shallow frictional heterogeneity, Nature Geosci. doi: 10.1038/NGEO1835.
- Winberry, J. P., S. Anandakrishnan, D. A. Wiens, and R. B. Alley (2013). Nucleation and seismic tremor associated with the glacial earth-

- quakes of Whillans Ice Stream, Antarctica, Geophys. Res. Lett. 40, 312-315, doi: 10.1002/grl.50130.
- Zecevic, M., G. Daniel, and D. Jurick (2016). On the nature of longperiod long-duration seismic events detected during hydraulic fracturing, Geophysics 81, no. 3, KS109-KS117, doi: 10.1190/ GEO2015-0524.1.
- Zigone, D., C. Voisin, E. Larose, F. Renard, and M. Campillo (2011). Slip acceleration generates seismic tremor like signals in friction experiments, Geophys. Res. Lett. 38, L01315, doi: 10.1029/ 2010GL045603.

Chenyu Li Zhigang Peng School of Earth and Atmospheric Sciences Georgia Institute of Technology Atlanta, Georgia 30332 U.S.A. lchenyu@gatech.edu

> Zefeng Li Seismological Laboratory California Institute of Technology Pasadena, California 91125 U.S.A.

Chengyuan Zhang State Key Laboratory of Geomechanics and Geotechnical Engineering Institute of Rock and Soil Mechanics Chinese Academy of Sciences Wuhan 430071, China

> Nori Nakata School of Geology and Geophysics University of Oklahoma Norman, Oklahoma 73019 U.S.A.

Tim Sickbert Boone Pickens School of Geology Oklahoma States University Stillwater, Oklahoma 74078 U.S.A.

Published Online 1 August 2018